Grid History: A Geostationary Satellite Technique for Estimating Daily Rainfall in the Tropics

DAVID W. MARTIN AND MICHAEL R. HOWLAND*

Space Science and Engineering Center, University of Wisconsin-Madison, Madison, WI 53706

(Manuscript received 12 May 1984, in final form 1 August 1985)

ABSTRACT

A new technique is described for estimating daily rainfall by means of visible and infrared geostationary satellite imagery. It is designed for the tropics and warm-season midlatitudes. Because it operates on a grid of points and measures time changes at these points, the technique has been named "grid history."

It is assumed that at any grid point in some image belonging to a sequence, by means of spectral, textural and evolutionary information, it is possible to classify instantaneous rain rate as nil, light, moderate or heavy. Then the total rainfall over a day is the sum over three classes of the product of frequency and class average rate.

The class average rates have been determined by least-squares multivariate linear regression of frequencies on observed rainfalls. The areas treated are South China Sea, India, Arabian Sea, tropical North Atlantic Ocean and Amazonia. Inland India had the lowest (driest) class average rates (coefficients), coastal India the largest (wettest) coefficients. Differences in coefficients were least for the Arabian Sea and Atlantic Ocean. There the class average rates were roughly zero (by definition), 1.5, 6 and 15 mm h^{-1}. For the strongly convective rain regimes treated here, it was found to be important to "look" at the area at least once per hour. A loss of accuracy in estimates over land apparently was due to unexpectedly large terrain and synoptic effects. Best-circumstance estimates of daily rainfall for an area 100 km on a side should be within a factor of 2 of true rainfall.

1. Introduction

The main impetus for designing a new technique for the measurement of tropical rainfall came from a field project, the 1979 Summer Monsoon Experiment (S-MONEX; Fein and Kuettner, 1980). At the heart of the Arabian Sea component of the S-MONEX was the onset of the southwest monsoon. Wind observations in unprecedented numbers showed that the onset in 1979 took place over a period not longer than ten days, and that this change was linked to a cyclonic storm of near hurricane strength.

It is to be expected that changes in patterns of rainfall would have paralleled (on smaller scales) changes in the low-level winds. Then a comparable description of the rains of the onset would require information over periods as short as a day, over distances as small as 100 km and of an accuracy sufficient to reveal such effects of synoptic scale systems as depletion of water vapor and warming by release of latent heat. We estimate that, on scales of one day and 100 km, this would require accuracy to within a factor of 2 of true rainfall. Unfortunately, over the Arabian Sea during summer MONEX, gage measurements, however good they might have been individually, numbered less than a dozen per day.

The implications of these circumstances are twofold: 1) only observations of the Indian Ocean Geostationary Operational Environmental Satellite (GOES-IO) simultaneously satisfy sampling and coverage requirements; 2) data from both channels (visible and infrared) probably are needed. From intensive observations of rain in other parts of the tropics (e.g., Houze and Hobbs, 1982; Cotton, 1982), we infer that it is important to account for warm as well as cold-cloud rain, layered as well as convective rain. From experience with satellite rain estimation techniques, we conclude that to process efficiently the volume of data available from GOES-IO, some automation is needed. These conditions have led us to develop a new satellite rain estimation technique.

For reasons which will become apparent later, the technique is called "grid history." Martin and Howland (1982) briefly described it and demonstrated its value in mapping the areas of light and heavy rainfall. A second paper (Martin and Howland, 1984) presented maps of daily Arabian Sea rainfall through the onset. The present paper provides a full description of the technique, including the procedure followed for estimating rainfall, applications in different regions, and the accuracy expected for the estimates.

2. Method

The grid history technique is based on the following five premises: 1) In most places rain is a rare event. 2)

* Current affiliation: Global Weather Central, Offutt Air Force Base, Nebraska.

Satellite data are redundant; i.e., rain-producing systems (rain cells) are much larger than a GOES visible or infrared pixel. 3) The two wavelengths contain complementary information on rainfall. 4) For both channels (see Barrett and Martin, 1981, pp. 102–23; also Lovejoy and Austin, 1979), brightness is the primary source of information on rainfall. Brightness thereby constitutes a coarse screen for rainfall. Further information, in rough order of importance, is contained in structure (including size), texture, and rates of change (both size and brightness). 5) Sequences of visible and infrared satellite images contain information sufficient to distinguish between at least four classes of rain rate.

Here, structure refers to macroscales: patterns of brightness the size of a cumulonimbus cloud and larger. It includes the size of a cumulonimbus cloud and other large rain clouds; also, the organization of rain clouds into systems such as squall lines, rainbands and cyclones. Texture refers to microscales: patterns of brightness internal to a cumulonimbus cloud or of scales smaller than a typical cumulonimbus cloud.

The technique is explained in terms of a typical problem, that of estimating daily rainfall of a convective nature. We suppose that geostationary satellite visible/infrared images are available at hourly intervals. Daily rainfall at a point within a grid covering the area of interest can be represented as

$$R = r(1) + r(2) + \cdots + r(24) \qquad (1)$$

where $r(i)$ is the rainfall for the (i) hour of the day and R is the daily rainfall. But only three non-zero rain classes (light, moderate, heavy) can be resolved at any given hour. Therefore, (1) can be expressed as

$$R \cong \hat{R} = r_1 f_1 + r_2 f_2 + r_3 f_3 \qquad (2)$$

where f_j is the number of times over 24 h that the (j)th rain class was assigned and $\hat{R}$ indicates an estimate. Over the area and period of the estimation, r_j is the constant rainrate assigned to the (j)th rain class.

The form of (2) suggests linear multiple regression of rain-class frequency f on observed daily rainfall R as an efficient way of determining the values of the r_j's. If we add a constant offset r_0, (2) becomes

$$\hat{R} = r_0 + r_1 f_1 + r_2 f_2 + r_3 f_3. \qquad (3)$$

The procedure followed for assignment of rain classes is outlined in Fig. 1. Computer functions are on the left side of the diagram; meteorologist functions are on the right side; time runs from top to bottom. In test cases already processed the "computer" has been the interactive video display device McIDAS (Man-computer Interactive Data Access System; Suomi et al., 1983) of the University of Wisconsin–Madison. Other programmable devices would do as well so long as they allowed a) display of sequences of satellite images, b) pairing of visible and infrared images, c) graphical overplotting both of coastlines, rivers or other primary landmarks and of rain-class assignments, d) cursor identification of particular points in an image, and e) access to digital image data.

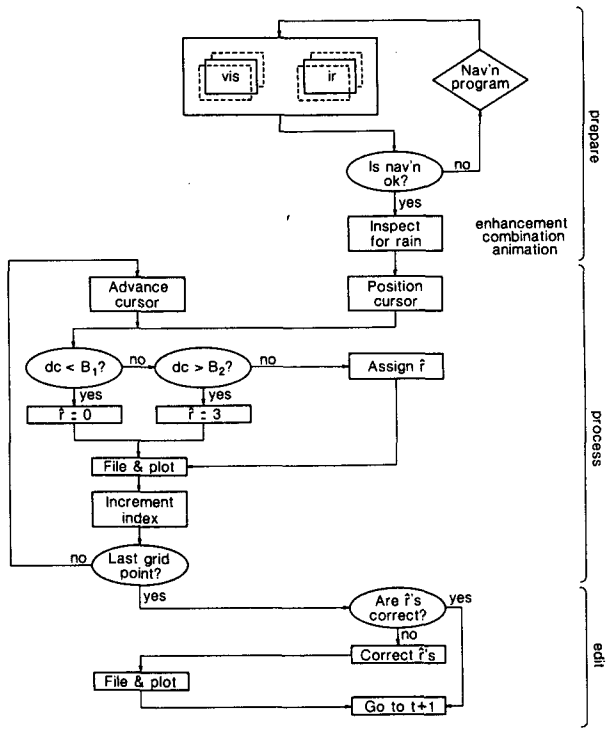

FIG. 1. Flow chart for the grid history scheme. Computer functions are on the left side, human functions on the right. Nav'n stands for navigation; dc is digital count; B_1 and B_2 are, respectively, warm (dark) and cold (bright) thresholds of digital count brightness; $\hat{r}$ is assigned rain class; 0, 1, 2, 3 representing nil, light, moderate and heavy rainrates, respectively.

First, by reference to landmarks, the image navigation (earth location, including registration of images) is checked. If errors are more than a small fraction of the grid spacing, the navigation is corrected. Second, through animation and other tools such as enhancement and/or color combination of visible and infrared images, the meteorologist develops a mental picture of the rain system structure. (This may be sketched on the face of the video monitor.)

The meteorologist proceeds to the processing stage by positioning a cursor at the upper left corner of the grid on the first image of the sequence. The rain estimation program is then invoked. This consists of several loops of more or less complexity depending on whether both visible and infrared data are present. If only visible data are present, the sequence is as follows:

1) The computer locates the picture element (pixel) closest to the cursor latitude and longitude.

2) It compares the pixel value against a low (dark) threshold. If the pixel is the same or darker, a nil-rain class is immediately assigned to that grid point, the class value is plotted on the television screen and filed, and the computer moves the cursor to the next grid

point. If the pixel is brighter than the minimum threshold, the computer compares it against a high (bright) threshold. If pixel brightness exceeds this second threshold, a heavy-rain class is assigned and that value is plotted and filed. If not, the computer defaults to the meteorologist, prompting him to make a decision. The meteorologist, on the basis of brightness and other factors given previously, chooses a rain class. This rain class applies only to the grid point pixel at the time (to the nearest minute or so) of the satellite image or images. The meteorologist enters the decision (by a keystroke) and in so doing passes control back to the computer. This process is repeated with the computer advancing the cursor to the next grid point each time a decision has been registered until the grid is completed.

3) The meteorologist inspects the field and corrects any mistakes. He then steps to the next image and repeats the procedure.

Not shown in Fig. 1 is a secondary loop entered when the heavy-rain threshold is exceeded at a grid point. By measuring the trend of pixel brightness from the preceding image, this loop takes account of the decay of a rain system (e.g., see Scofield and Oliver, 1977). If the trend is toward marked darkening (20 brightness counts or more, which is roughly equivalent to a thickness change of 4 km or more), the rain-class assignment is dropped from heavy to moderate.

The procedure for an infrared image is similar to that of Fig. 1. The thresholds are, of course, different. A secondary loop is also entered when the infrared heavy-rain threshold is exceeded. When at least a 10°C warming occurs in the following image, the heavy-rain assignment is reduced to moderate. (A 10°C warming corresponds to about a 2-km decrease in cloud top height.) In the case where visible and infrared images are present together, a loop is added which uses both channels of data to test for cold clouds with a moderate visible brightness. Even though the single channel no-rain threshold may have been exceeded, this loop eliminates some thick cirrus and cumulonimbus anvil edges by assigning these points a nil-rain class.

No-rain thresholds are like those used by Griffith et al. (1978) and Stout et al. (1979) for Florida and tropical east Atlantic convection. Initially, no-rain thresholds were set at 172 digital counts for visible and 160 digital counts for infrared. During processing it was found that the Arabian Sea required a higher no-rain infrared threshold (180 was used) to account for large areas of "dry" cumulonimbus anvils and upper jet-level cirrus. The heavy-rain thresholds were chosen after sampling the deepest convection over several days. In the case of the Arabian Sea, they were set at 220 for infrared and 240 for visible images. The choice of thresholds is intended to be flexible and can be tailored to the geographical area and season for which estimates are to be made.

In order for a single set of visible thresholds to apply in time and space, visible brightness is normalized using an empirical relationship for brightness correction as a function of the solar zenith angle. The relationship was developed by LeBlanc (1980) for Atlantic Intertropical Convergence Zone clouds in GOES visible images. It is applied at each grid point as long as the zenith angle is less than 60°. The normalization in the tropics allows processing of the visible channel within ±3 h of local noon. The remaining 17 hours of the day are processed on the infrared channel, although low-sun visible images are still used as a reference by the meteorologist.

Within the limits of any particular geostationary satellite data set, image resolution and interval, together with the spacing of the grid points, are selected to match the scale of the rain cells which are expected to occur over some geographic area of interest. Experience suggests these guidelines: 1) image resolution should be not less than one-fourth the diameter of the smallest raincell of significance; 2) grid spacing should be not more than twice the diameter of the smallest raincell of significance; 3) image interval should be not more than one-half the lifetime of the most transient raincell of interest. The grid domain and period of estimate are chosen so that constant coefficients are reasonable.

3. Calibration

The procedure outlined here and diagrammed in Fig. 1 allows the assignment of rain classes in a gridded pattern over any region and time interval for which satellite images are available. To convert these rain class assignments to rain amounts, the coefficients r_0, r_1, r_2, and r_3 must be determined. We refer to this process as calibration and include as part of it an evaluation of the accuracy of $\hat{R}$.

Calibration was accomplished through the use of special data sets consisting of 24 h rain class frequencies matched to simultaneous, coincident gage observations of rainfall. Except as noted below, the calibration was blind in the sense that rain-class assignments were made in ignorance of gage rainfall amounts.

The calibration procedure consisted of three main steps: 1) For each time interval a rain class (determined as in section 2 from one or both channels of satellite imagery) was assigned over the gage location. 2) Occurrences of each rain class were summed over 24 h. 3) Coefficients were calculated through least-squares multivariate linear regression of frequencies against daily gage rainfall. Statistics calculated during regression included correlation coefficients, regression offset, and the standard error of estimate based on the regression sample. The main deviation from this procedure was the occasional determination of frequencies by interpolation from grids rather than direct assignment over gage locations. Frequencies were interpolated when gage locations were not available at the time im-

ages were processed, or when a large number of gages made direct assignment impractical.

a. Arabian Sea

The calibration data set over the Arabian Sea consisted of eight consecutive days of hourly visible and infrared imagery at 4 km resolution from GOES-IO and gage rainfall from five Soviet research ships and four islands (Fig. 2). Navigation accuracy was about 4 km for the visible imagery and about 12 km for the nighttime infrared. The calibration period began on 11 June; it coincides with the 1979 monsoon onset over the Arabian Sea.

Information on the exposure of the gages shown in Fig. 2 is not available. However, because the islands are atolls and the ships were outfitted for research, it is believed that these gage measurements are representative of local rainfall. (See Kilonsky and Ramage, 1976.) Unfortunately, the ships were on station only for the first three days of the calibration period. Additional information on data is contained in the Appendix.

Coefficients for the Arabian Sea and regression statistics are shown in Table 1. Scatterplots of frequency versus gage rain for light-, moderate- and heavy-rain classes are shown in Fig. 3a, b, c. If four rain classes actually can be distinguished, the cloud of points in each of the aforementioned parts should—by Eq. (3)—exhibit a progressive change in slope. In the case of Fig. 3, because of the plotting convention used, the change should be towards flatter slopes from light through heavy rain classes [parts (a) through (c)]. Indeed that is the case.

Also shown in Fig. 3 is a scatterplot of measured versus estimated daily rainfall, for the calibration days only. The standard error of estimate was 12.8 mm d^{-1}. (The mean was 16.5 mm d^{-1}.) The regression relationship accounted for 43% of the variance in rainfall. Of the 47 rainfall estimates resulting from the application of (3), 79% are within a factor of 2 or ±5 mm of rainfall reported at the corresponding gage.

Heavy rainfall for the four island stations on the second day of the calibration period accounted for a large part of the standard error of estimate. When this day was removed from the data set (not shown), more of the variation in rainfall was explained by the regression and the coefficients were a bit drier. Interpolation of the frequencies from grid to gage location may have contributed to the discrepancy on this day, as strong gradients in rain-class frequencies existed near the islands.

Using (3), we estimated daily rainfall at the island stations on each of two test days, 19 and 20 June. In this case, satellite rain classes were assigned at the locations of the gages. The results are shown in Fig. 4.

There is a tendency toward underestimation of heavy

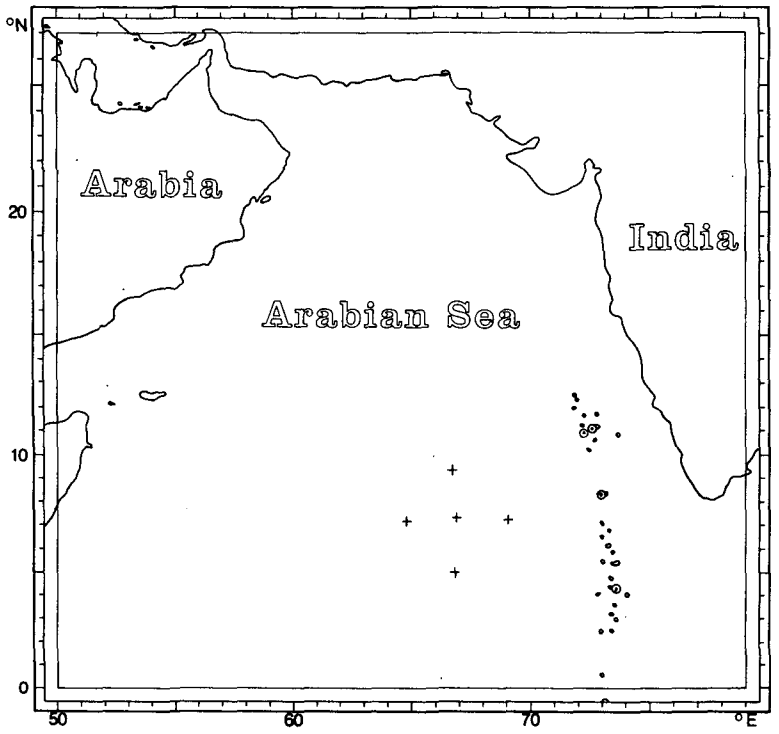

FIG. 2. Arabian Sea raingages and grid domain. Locations of island gages are marked by circles; ship gages by crosses. The thin solid line connects points on the perimeter of the grid domain.

TABLE 1. Calibration results.*

Data set	No. of cases	Individual rain class correlations			Multiple regression						
					Coefficients				Statistics		
		$\rho(f_1)$	$\rho(f_2)$	$\rho(f_3)$	r_0	r_1	r_2	r_3	ρ	ρ^2	ϵ
Arabian Sea	47	0.44	0.62	0.34	0.5	0.6 (1.5)	8.7 (8.8)	17.6 (19.9)	0.69	0.43	12.8 (13.1)
Arabian Sea with test days	55	0.49	0.68	0.34	4.1	0.5 (1.2)	9.9 (9.9)	17.3 (19.3)	0.73	0.50	12.3 (12.4)
Coastal India	124	0.54	0.65	0.32	3.5	3.7 (4.7)	21.7 (21.4)	11.4 (10.6)	0.67	0.43	29.9 (29.9)
Inland India	446	0.36	0.47	0.14	0.2	1.3 (1.4)	5.1 (5.2)	0.6 (0.6)	0.49	0.24	4.6 (4.6)
GATE	59	0.73	0.75	0.50	−0.8	1.8	5.0	9.3	0.86	0.74	7.1
Marajo Island	84	0.63	0.69	0.47	0.6	1.6 (1.7)	4.5 (4.6)	7.8 (7.6)	0.74	0.54	5.3 (5.3)

* The symbols ρ and ϵ denote correlation coefficient and standard error of estimate, respectively. The units for r_0 are mm d^{-1}. Coefficients (r_1, r_2 and r_3) have all been converted to units of mm h^{-1}. Numbers in parentheses show results of regression through the origin (offset forced to zero).

rainfalls and overestimation of light rainfalls for the test days. Otherwise, the correlation is like that found for the calibration days. When the data from both sets are combined, the coefficients for (3) are little changed, but the larger sample explains nearly 50% of the variance in rainfall and has a stronger correlation to the

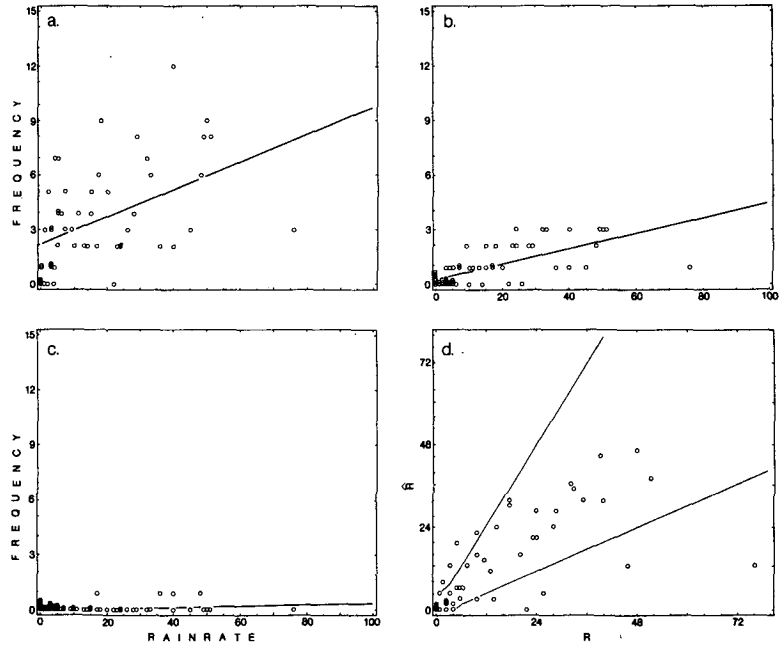

FIG. 3. Scatterplots for the Arabian Sea. Panels a, b and c show gage rain vs. rain class frequency for, respectively, light, moderate, and heavy classes. Counting the six zero rainfalls, there are 55 points (corresponding to 55 separate gage measurements of daily rainfall) in each part. Each point is represented by a circle. For each part the line of least-squares linear regression (with rain as the dependent variable) also is shown. Panel d shows gage rainrate R vs. estimated rainrate $\hat{R}$. The value of $\hat{R}$ was calculated from the calibration frequencies using the Arabian Sea coefficients (through the origin; Table 1). Sloping lines are confidence limits. Above R = 10 mm d^{-1} they represent a factor of 2 of R; below R = 10 mm d^{-1} they represent $R \pm 5$ mm d^{-1}. Rain rates are in units of millimeter per day.

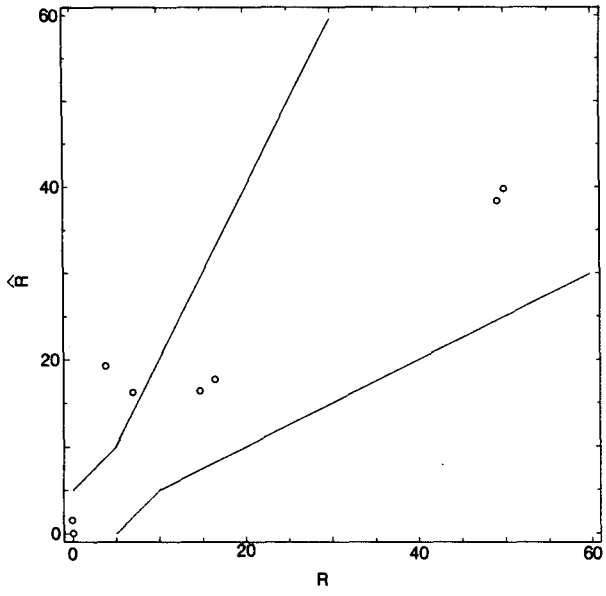

FIG. 4. Satellite-estimated vs gage-measured rainrates (mm d^{-1}) for the island stations of the Arabian Sea, test cases. Otherwise as in Fig. 3d.

gage data (see Table 1). Part of the reason for the improved fit on the two test days may be that rain-class frequencies were assigned directly over the gage locations for these days. (The test data were processed after the gages had been located.) Adding eight more reports to the regression tended to balance the heavy rain reports of the four islands on 12 June, adding confidence to the stability of the coefficients over the Arabian Sea.

b. *India*

Rainfall reports over India are abundant in comparison with the Arabian Sea. Over India rainfall is known to be highly variable (Parthasarathy, 1960, Raghaven, 1964, Staff Members, 1964). It may be different from rainfall over the Arabian Sea. For these reasons, a separate calibration was made for India. Rain-class frequencies are from the same set as for the Arabian Sea calibration. As in that calibration, frequencies were interpolated from grid point to gage location. For the Indian data, we used a simple three-directional spline interpolation. The procedure weighted the four grid points surrounding a station report based on their relative distance from the gage location. Stations not within 25 km of any grid point were rejected. Interpolation probably contributed significantly to the variance between observed and estimated values of rainfall.

It was anticipated (e.g., Das, 1968) that the rains of the western coast would be different from those of the interior of India. Therefore, for the calibration, India was divided by the natural climatic boundary along the crest of the Western Ghats into coastal and inland regions. The calibration domain was limited to India north to the 27th parallel and east to the 79th meridian. There were 124 coastal and 446 inland daily station reports available for the regression analysis; the means were, respectively, 22.2 and 1.2 mm d^{-1}.

Calibrations for the two regions are shown in Table 1. The coastal region had noticeably "wetter" coefficients than the Arabian Sea. The inland coefficients were drier than either the coastal or the Arabian Sea coefficients and inland correlations were lower. Both the inland and coastal regions did poorly in defining a coefficient for the heavy rain class, possibly due to a small number of heavy-rain assignments. For the inland area, rainfall was assigned too often. Apparently, land–sea differences, elevation of the land surface, and airflow relative to relief played a larger and more complicated role than had been anticipated in the assignment of rain classes over India.

c. *GATE region*

Similar calibrations were made for three locations elsewhere in the tropics. One of these was in the eastern Atlantic Ocean, site of the Global Atmospheric Research Program Atlantic Tropical Experiment (GATE). Hourly Synchronous Meteorological Satellite (SMS) images for the GATE Phase III A/B scale research ship array were available for 2 September and for 4–6 September 1974. The images had the same resolution and approximate navigation accuracy as those used for the Arabian Sea. Rain-class frequencies were assigned at the reported locations of ships. The assignments were made by a meteorologist (Howland) who had no prior knowledge of GATE rainfall or familiarity with the cloud systems for these four days. The resulting 59 sets of rain-class frequency and ship-gage reports were used to determine the GATE coefficients and regression statistics shown in Table 1 and in Fig. 5.

The coefficients are drier than those for the Arabian Sea. As for the Arabian Sea, there is a marked separation in coefficients for the three rain classes. Over 84% of the stations had predicted rainfall within a factor of 2 or ±5 mm of the actual observations. (Mean rainfall was 9.0 mm d^{-1}.) Almost 75% of the variance in observed rainfall was captured by the regression relationship.

d. *Marajo Island, Brazil*

The second supplementary calibration was made at a coastal equatorial site, Marajo Island. This calibration was compromised by flaws in the data, which became apparent in the course of the analysis. It is presented, nevertheless, because it provides information on a rain regime that otherwise would not be represented.

Marajo is an island at the mouth of the Amazon River. Centered at 1°S, 50°W, it is roughly 300 km in length, 200 km in width and flat. Overall, rainfall is high on the island, about 2500 mm per year (Ratisbona, 1975). It varies diurnally (Kousky, 1980) and seasonally

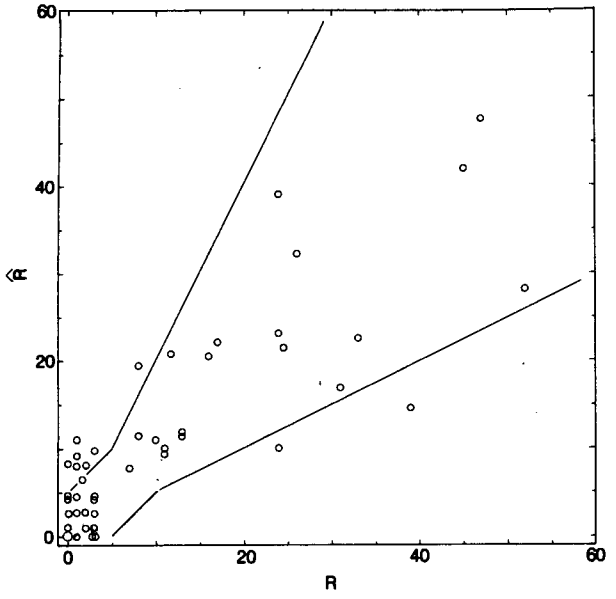

FIG. 5. Satellite-estimated vs. gage-measured rainrates (mm d^{-1}) for the ships of GATE, calibration cases. There are 15 points at (0, 0). Otherwise as for Fig. 3d.

(Ratisbona, 1975; Nechet, 1981); also—despite the lack of relief—spatially (Souza et al., 1980).

Over the last two decades, several agencies of the government of Brazil or state of Para have operated raingages on Marajo Island. With as many as 25 gages (including a few recording gages) over its 50,000 km^2 area, Marajo has the highest gage density of any part of the Amazon (E. Cutrim, personal communication 1983).

Gage rainfalls provided by Dr. Cutrim were compared with rain class frequencies for six days of 1978, three from April (wet season) and three from September (dry season). For these days there were 23 gages operating on Marajo. A gage from Belem, opposite the Island, was added to that set. The distribution of the 24 gages is shown in Fig. 6. Strip charts from recording gages were available for four stations during the wet season, three during the dry season. These proved to be valuable as checks on the daily observations. Further information on data and details of the processing are contained in the Appendix.

Results appear in Fig. 7 and Table 1. The scatterplots (Fig. 7) show little difference between wet and dry seasons. Therefore, in calculating statistics these have been combined. The regression correlation of daily rain class frequency with daily rainfall was 0.74. The standard error of estimate was 5.3 mm; mean daily rainfall was 3.7 mm.

e. South China Sea

The last and least successful calibration was made in the context of comparing the performances of satellite rain estimation techniques over the South China Sea and its southern littoral. This experiment covered ten days, beginning on 11 December 1978.

Rainfall measurements were obtained (by Mr. Songkran Agsorn) from the governments of Indonesia, Malaysia, Singapore, and Thailand. Stations on the Malay peninsula and the islands of Sumatra and Borneo proved to be located mostly along the coasts. A few stations were scattered across islands between Borneo and Sumatra. Land gages totaled 40 but not all reported on any given day. Rainfall also was measured

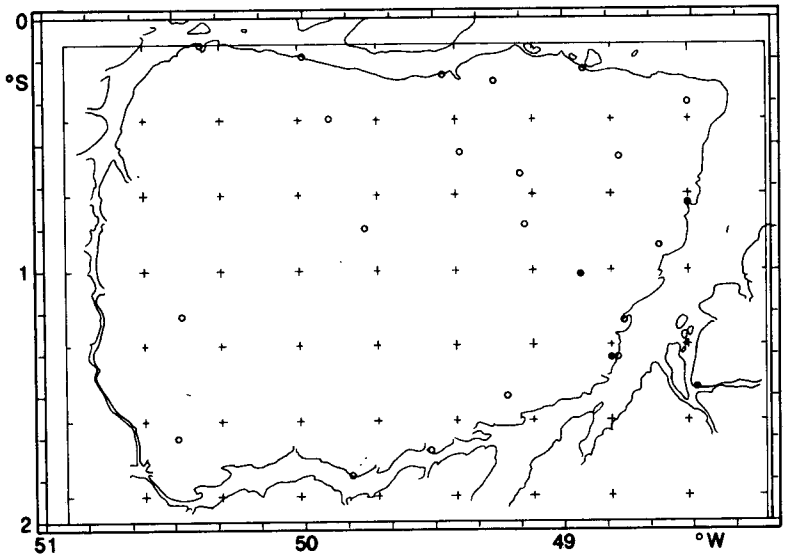

FIG. 6. Marajo Island raingages. Simple gages are shown by open circles, recording gages by solid circles. Also shown (except for the bottom tier of points) is the grid over which rain classes were assigned.

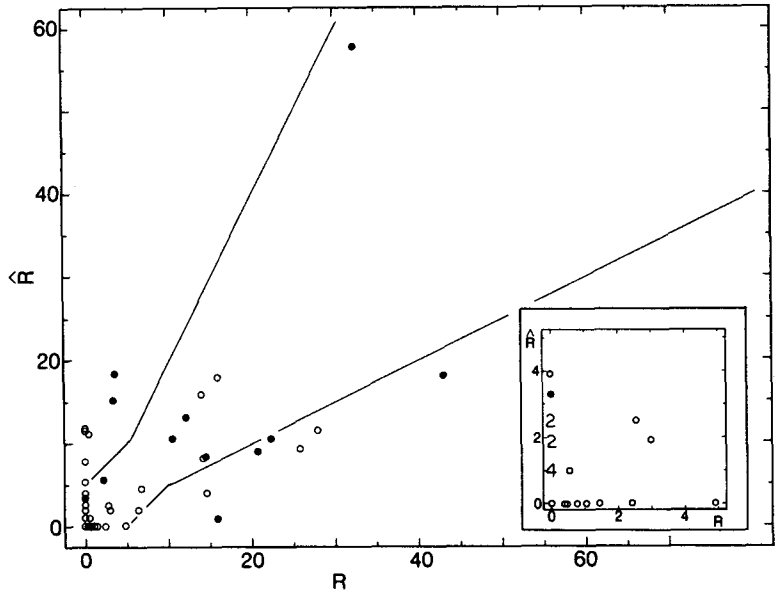

FIG. 7. Satellite-estimated vs gage-measured rainrates (mm d^{-1}) for Marajo Island, calibration cases. Open circles are wet season cases; closed circles, dry season cases. The part of the domain within 5 mm d^{-1} of the origin is enlarged at the lower right. Otherwise as for Fig. 3d.

aboard three Soviet research ships stationed in the South China Sea.

At Bintulu, on the north coast of Borneo, the Massachusetts Institute of Technology operated a meteorological radar of 5 cm wavelength (Houze et al., 1981a). Only the seaward part of each horizontal scan provided useful data. For present purposes, sampling within the seaward part of the scan was limited to ranges of 70 km and less. Reflectivities were converted to rainrates through a GATE (eastern Atlantic) Z–R relation, and accumulated over 3 h periods. These data were provided at 4 by 4 km resolution by Mr. S. Geotis of the Massachusetts Institute of Technology (personal communication, 1982). Before being compared to satellite rain-class frequencies, they were degraded to 0.1° by 0.2° (10 by 20 km) resolution.

In 1978, the South China Sea was viewed by one geostationary meteorological satellite, that of Japan. The interval between images for this satellite (GMS) is usually 3 h. Because the area to be covered was large, the resolution of both visible and infrared images was degraded to 10 km. Navigation was a serious problem with these otherwise excellent data. Even after image-by-image landmark registration, errors in geographic location ranged upward to 20 km.

Three of the ten days were reserved for verification. Gage and radar ground truth data were treated in separate calibrations. The results are given in Table 2. Except for the offset, coefficients calculated from gage rainfalls were much higher than those calculated from radar rainfalls.

The calibrations were then applied to the three additional days of satellite rain class frequencies. Predicted rainfalls were compared with both gage and radar-observed rainfalls. These results are also summarized in Table 2. The bias was negligible only in the case of gage-calibrated estimates compared with gage rainfalls. The correlation coefficient approached significance only in the case of radar-calibrated estimates compared with gage rainfalls.

TABLE 2. South China Sea calibration.*

	Regression coefficients					Test results: Gage		Test results: Radar	
Calibration set	r_0	r_1	r_2	r_3	ϵ	ρ	Bias	ρ	Bias
Gage	2.4	1.0	5.0	7.7	22.3	0.18	1.0	0.14	1.5
Radar	3.0	0.3	0.4	2.8	10.2	0.37	0.2	0.16	1.2

* The symbols ρ and ϵ and the units for r_0, r_1, r_2 and r_3 are as in Table 1.

The pattern of the bias (radar calibration giving less rain than the gage calibration) indicates a difference in the character of the rains sampled by the gages and the radar. Gage rain systems, which occurred mainly over land, tended to produce heavier rains. Gage coefficients (converted to common units) are like those for GATE and Marajo Island.

Ramage (1971, p. 139ff), Houze et al. (1981b), Johnson and Priegnitz (1981), and others have remarked on the complexity of the rains of this region. Probably this complexity contributes to the poor performance of the grid history technique in this application. Certainly poor navigation and degraded resolution of images are contributing factors. Most importantly, because much of the forcing occurred on a diurnal time scale, 3 h sampling failed to capture part of a large and important class of convective rains.

4. Consistency among analysts

Experiments were conducted to measure consistency in rain class assignments from one person to another. These experiments involved independent processing of the same image (or image sequence). Two of the four test cases were from the sequences presented previously. Of the remaining two, one concerned the near-equatorial Arabian Sea well before onset and the other concerned the Texas–Louisiana Gulf Coast.

The results, in terms of class frequencies, are summarized in Table 3. Only the South China Sea comparison involved a person who had not helped to develop the technique. Compared to the other three cases, the difference there was very large. Differences between the authors were, at worst, marginally significant by the chi-square test. They were largest for the infrared-only cases; smallest for the (single) visible-only case (which had the benefit of a preview of the infrared). In one case (Gulf Coast) the comparison was extended to include spatial agreement. There, 85% of all assignments were identical. No assignment pairs differed by more than one class.

5. A test of classification by threshold

A series of simple tests were conducted (using the GATE data set described previously) to evaluate the subjective aspect of the technique (i.e., the contribution of the meteorologist). Rain was assigned at GATE ship locations in three rain classes determined solely by brightness thresholds. The lower and upper thresholds (rain/no-rain and heavy-rain) were those established for the grid history technique in its application to the Arabian Sea. The intermediate threshold was variable. Values were selected to separate rain classes, maximize correlations, and minimize standard errors of estimate.

The thresholds for infrared only and those for visible and infrared together are shown in Table 4. A summary of the results for the threshold classification is shown in Table 5. The original grid history results for the GATE data set are given in Table 5 for comparison.

The effect of a simplification to two and finally one non-zero rain class is also shown in Table 5. This was achieved by combining rain classes, first the moderate- and heavy-rain classes, and then all three rain classes.

When only the infrared channel was used, 180 digital counts worked better as a rain/no-rain threshold than

TABLE 3. Rain class assignment comparison.*

a. Arabian Sea–day 79130

Rain class	Infrared OP1	Infrared OP2	Visible OP1	Visible OP2	Both channels OP1	Both channels OP2
Nil	1221	1214	1271	1275	1270	1280
Light	59	49	21	18	19	14
Moderate	26	36	13	9	16	10
Heavy	5	12	6	9	6	7
χ^2	8.9		2.4		5.6	

b. Arabian Sea–day 79164

Rain class	Infrared OP1	Infrared OP2
Nil	669	637
Light	65	85
Moderate	16	25
Heavy	4	7
χ^2	10.8	

c. Gulf Coast–day 79188

Rain class	Both channels OP1	Both channels OP2
Nil	482	499
Light	273	272
Heavy	61	45
Total	816	816
χ^2	4.8	

d. South China Sea–day 78350

Rain class	Both channels OP3	Both channels OP2
Nil	615	690
Light	588	686
Moderate	487	384
Heavy	200	130
Total	1890	1890
χ^2	71.7	

* $\chi^2_* = 7.82$ and 11.34 at the 0.05 and 0.01 significance level, respectively, with three degrees of freedom. If $\chi^2 < \chi^2_*$, we accept the null hypothesis that both samples come from the same population. OP stands for operator.

TABLE 4. Automated estimation thresholds.

Infrared only thresholds		Visible and infrared thresholds	
Rain class	Threshold	Rain class	Threshold
Nil	$I \leq 180$	Nil	$V \leq 172$
Light	$181 \leq I \leq 207$	Nil	$V \leq 195$; $I \geq 180$
Moderate	$208 \leq I \leq 217$	Light	$172 \leq V \leq 214$
Heavy	$I \geq 218$	Moderate	$215 \leq V \leq 239$
		Heavy	$V \geq 240$

* V and I refer to normalized-visible and infrared digital counts, respectively.

did 160 digital counts. This supports experience for the Arabian Sea. Only the light and moderate rain classes were statistically significant. Furthermore, even though the moderate-rain class was significant with better than 95% confidence, the two-rain-class scheme was only marginally better than the straight rain/no-rain scheme.

With visible imagery added to the threshold scheme, regression skill increased considerably. Three non-zero rain classes were statistically significant. When rain classes were merged, especially from two to one, regression skill was lost.

Grid history estimates explained 11% more of the variance in daily ship rainfall and decreased the standard error of estimate by 18% in comparison to the best threshold classification scheme. Thus, despite the surprising skill of the multiple-channel threshold classification, the meteorologist added a substantial share of additional information.

6. Discussion

A method has been described for estimating daily, storm-scale rainfall in those parts of the tropics viewed by geostationary meteorological satellites. The method assumes that visible images complement infrared images, rain is a rare event, screening (by brightness, structure, texture and behavior) isolates areas of probable rain, and that within each such area three classes of rain rate can be distinguished. Rainfall is estimated on a grid by means of a linear regression equation in which the independent variables are rain-class frequencies. These are determined interactively, from a movie display of satellite imagery.

The method was tested in the South China Sea, India, the Arabian Sea, the tropical north Atlantic Ocean and lower Amazonia. Each test involved the determination of coefficients by least-squares regression of rain-class frequencies against gage rainfalls. In one case (South China Sea) radar rainfalls also were used.

Coefficients for coastal India were the largest (wettest); those for inland India were the smallest (driest). The differences apparently are related to local moisture content of the atmosphere and orographic influences on rain efficiency. These factors proved to be more important than had been anticipated in the design of the method.

With one exception, coefficients for each region increased from light through heavy-rain classes. The exception was India, where rainfall was highly variable and relatively few heavy-rain classes were assigned. In the "best case" results of the Arabian Sea and east Atlantic Ocean the neighbor-to-neighbor ratios of coefficients were 4 and 3, respectively. These ratios imply roughly a factor 10 difference between light and heavy rain rates.

Performance was affected most seriously by the interval between images. Not far behind in compromising results were errors in image navigation. These factors combined to produce poor results in the South China Sea experiment. There, as well as over India and lower Amazonia, complexity and variability of rain systems also compromised the quality of estimated rains.

Only two completely independent verifications were attempted. One, for the South China Sea, showed little

TABLE 5. Threshold classification.*

Data set	Number of rain classes allowed	Rain class correlation			Regression coefficients				Regression statistics		
		f_1	f_2	f_3	r_0	r_1	r_2	r_3	ρ	ρ^2	ϵ
Infrared only	3	0.66	0.45	0.07	0.00	2.12	4.48	—	0.70	0.47	10.0
Infrared only	2	0.66	0.44		−0.13	2.12	4.49		0.70	0.47	10.0
Infrared only (180 as threshold)	1	0.69			−0.33	2.35			0.69	0.47	10.0
Infrared only (160 as threshold)	1	0.64			−0.96	1.71			0.64	0.40	10.6
Visible and infrared	3	0.64	0.70	0.31	0.01	1.55	4.58	10.03	0.80	0.63	8.4
Visible and infrared	2	0.64	0.72		0.28	1.43	5.21		0.80	0.62	8.5
Visible and infrared	1	0.75			−0.13	2.28			0.75	0.55	9.2
Grid history	3	0.73	0.75	0.50	−0.80	1.80	5.00	9.30	0.86	0.74	7.1

* GATE rainfall averaged 9.8 mm with a standard deviation of 13.7 mm for the 54 daily ship reports over the four test days. Symbols are as in Table 1. The heavy-rain class for the three-class infrared-only case failed the test for statistical significance and therefore was not determined.

skill in estimates from 3 h imagery in which locations were known to ±20 km accuracy. The other, for the Arabian Sea, showed substantial skill in estimates from 1 h imagery in which locations were known to ±10 km (or better) accuracy. The latter test, together with calibration results for the Atlantic Ocean and Arabian Sea, suggests that if 1 h visible and infrared data are used, over-water estimates of daily rainfall averaged over areas $(100\ \text{km})^2$ in size should meet the standard set out in section 1, i.e., to be within a factor of 2 of the true rainfall.

For persons familiar with the technique, adding spectral data causes the results to converge. Where both channels are present, classification differences can be negligibly small. Not so encouraging is the indication that lack of skill is an additional reason for the poverty of the South China Sea estimates. This result underlines the importance of clear-cut decision standards.

One means for controlling inconsistencies in interpretation is to automate pattern recognition. An effort in this direction is described by Lee et al. (1984). More are needed. A simple threshold-only scheme was tested for the GATE region. Even when both infrared and visible data were used, skill was notably short of what had been achieved by the full grid history technique. Apart from extensions of the technique to other parts of the tropics, further calibration and testing are needed, especially in regimes of heavy rain. A network of recording raingages or a gage-calibrated digital radar would be of great value for such tests. Finally, the time has come to blend satellite visible-infrared data with satellite passive microwave data, perhaps following the radar-satellite approach of Bellon et al. (1980). By such means it may be possible systematically and reliably to map warm season rainfall over the continents.

Acknowledgments. S. G. Geotis and E. M. C. Cutrim provided data. B. G. Lee and S. Agsorn assisted in the data processing. A. M. Crowell and J. Edwards typed the manuscript, and B. B. Hinton reviewed an early version. These contributions are gratefully acknowledged. Funding was provided by the National Science Foundation under Grant ATM 7920850 and the National Oceanic and Atmospheric Administration under Grants NA-80-SAC-00742 and NA-84-DGC-00240.

APPENDIX

Processing Notes

a. Arabian Sea

Three hours of satellite imagery were missing on 11 June. On one day (13 June), over a 10 h period, the infrared sensor drifted toward saturation (an all black image). To salvage information from these images, a linear correction was applied which maintained constant temperature for the coldest cloud tops. Some warm cloud rain may have been missed during the last four hours of the drift. After the infrared sensor had been shut off for one hour, it provided good data through 20 June.

Rain class frequencies were assigned on a grid at ½° × ½° spacing for the first three days, and at 1° × 1° spacing for the remaining five days. Grid frequencies were interpolated (by hand analysis) to the gage locations. The three missing hours of 11 June and one missing hour of 13 June were accounted for by applying a linear correction to the frequencies. Forty-seven pairs of gage rainfall and rain-class frequency were then available for regression analysis.

b. Marajo Island

Images of the eastern Geostationary Operational Environmental Satellite (GOES) were processed at resolutions of 2 km (visible) and 4 km (infrared; oversampled across lines). For both infrared and visible data, the interval between images was ½ h. On each day, a part of the sequence was missing. For the dry season this came to four or five images and the gap was filled by weighting daily rain-class frequencies as $48/(48 - n)$, where n is the number of missing images.

For the wet season, n ranged from 10 to 16. Since the gaps were long compared to the lifetimes of the main rain systems, the wet season gaps could not be bridged by any simple method. Therefore, for the wet season, only gage/satellite pairs based on strip chart records (four stations) appear in the results presented previously. As individuals these pairs were given the same weight as the dry season pairs.

Rain classes were assigned for a grid encompassing all the gage stations (Fig. 6). The grid-point spacing was 0.3 deg latitude/longitude (33 km). The assignments were made as described in section 2, except that visible/infrared image pairs were displayed in pseudocolor and all assignments were made by one person (Martin). The grids of rain class were summed over 24 h (0730 to 0700 LST, 1030 to 1000 GMT) and corrected for missing images. These grids were contoured by hand. From the daily class frequency maps, rain-class values were read at each of the 24 gage stations and compared with gage observations of daily rainfall.

Poor agreement of rain classes and rainfall on two days led to a check of the wet season navigations. In one case a navigation error was partially corrected by means of new landmarks. In another case a mismatch in an infrared sequence was found and corrected. One correction was easily applied by shifting the relative position of the grids over the gages. The other required reassignment of rain class for the entire wet season day. This was done several months after the original processing and rain class assignments were made at the four recording stations rather than at grid points. Although the operator by that time had seen the strip charts, the recollection was faint and the stations were anonymous. Thus, it is believed that foreknowledge could not have had more than a modest influence on

the rain classes which were assigned. Both corrections produced stronger relationships between rain-class frequencies and rainfalls.

REFERENCES

Barrett, E. C., and D. W. Martin, 1981: *The Use of Satellite Data in Rainfall Monitoring,* Academic Press, London, 352 pp.

Bellon, A., S. Lovejoy and G. L. Austin, 1980: Combining satellite and radar data for the short-range forecasting of precipitation. *Mon. Wea. Rev.,* **108,** 1554–1566.

Cotton, W. R., 1982: Modification of precipitation from warm clouds—a review. *Bull. Amer. Meteor. Soc.,* **63,** 146–160.

Das, P. K., 1968: *The Monsoon,* National Book Trust, New Delhi, 168 pp.

Fein, J. S., and J. P. Kuettner, 1980: Report on the summer MONEX field phase. *Bull. Amer. Meteor. Soc.,* **61,** 461–474.

Griffith, C. G., W. L. Woodley, P. G. Grube, D. W. Martin, J. Stout and D. N. Sikdar, 1978: Rain estimation from geosynchronous satellite imagery—visible and infrared studies. *Mon. Wea. Rev.,* **106,** 1153–1171.

Houze, R. A., Jr., and P. V. Hobbs, 1982: Organization and structure of precipitating cloud systems. *Advances in Geophysics,* **24,** Academic Press, 225–315.

——, S. G. Geotis, F. D. Marks, Jr. and A. K. West, 1981a: Winter monsoon convection in the vicinity of north Borneo. Part I: Structure and time variation of the clouds and precipitation. *Mon. Wea. Rev.,* **109,** 1595–1614.

——, ——, ——, D. D. Churchill and P. H. Herzegh, 1981b: Comparison of airborne and land-based radar measurements of precipitation during Winter MONEX. *J. Appl. Meteor.,* **20,** 772–783.

Johnson, R. H., and D. L. Priegnitz, 1981: Winter monsoon convection in the vicinity of north Borneo. Part II. Effects on large-scale fields. *Mon. Wea. Rev.,* **109,** 1615–1628.

Kilonsky, B. J., and C. S. Ramage, 1976: A technique for estimating tropical open-ocean rainfall from satellite observations. *J. Appl. Meteor.,* **15,** 972–975.

Kousky, V. E., 1980: Diurnal rainfall variation in northeast Brazil. *Mon. Wea. Rev.,* **108,** 488–498.

Krishnamurti, T. N., D. Ardanuy, V. Ramanathan and R. Pasch, 1979: Quick Look Summer MONEX Atlas, Part II. The Onset Phase. Report No. 79-5, Department of Meteorology, Florida State University, Tallahassee, 32306, 205 pp.

——, P. Ardanuy, Y. Ramanathan and R. Pasch, 1981: On the onset vortex of the summer monsoon. *Mon. Wea Rev.,* **109,** 344–363.

LeBlanc, A. M., 1981: An objective technique for the analysis of cloud populations. Development of Satellite Image Processing Techniques for the First GARP Global Experiment. Final Report on NASA Contract NAS5-23462, Space Science and Engineering Center, Madison, Wisconsin, 221–275.

Lee, B. G., R. T. Chin and D. W. Martin, 1985: Classification of rain cells in satellite imagery. *IEEE Trans. Geosci. Remote Sensing* GE-23, 315–324.

Lovejoy, S., and G. L. Austin, 1979: The delineation of rain areas from visible and IR satellite data for GATE and mid-latitudes. *Atmosphere-Oceans,* **17,** 77–92.

Martin, D. W., and M. R. Howland, 1982: Rainfall over the Arabian Sea during the onset of the 1979 monsoon. *Nature,* **300,** 628–630.

——, and ——, 1984: Daily Arabian Sea rainfall during the onset of the 1979 monsoon. *Papers in Meteorological Res.* (Taipei)

Nechet, D., 1981: *Aplicacao de Normal Climatologica em Planejamento a Longo Prazo.* Servico Regional de Protecao ao Voo, Belem, Brazil.

Parthasarathy, K., 1960: Some aspects of the rainfall in India during the southwest monsoon season. *Monsoons of the World* (S. Basu et al., Eds.), Hind Union Press, New Delhi, 185–194.

Ratisbona, L. R., 1976: The climate of Brazil, *World Survey of Climatology,* **12,** Elsevier, 219–269.

Raghaven, K., 1964: Influence of the Western Ghats on the monsoon rainfall at the coastal boundary of the peninsular India. *Indian J. Meteor. Geophys.,* **15,** 617–620.

Ramage, C. S., 1971: *Monsoon Meteorology,* Academic Press, 296 pp.

Scofield, R. A., and V. J. Oliver, 1977: A Scheme for Estimating Convective Rainfall from Satellite Imagery. NOAA Tech. Memo. NESS 86, Washington, D.C., 47 pp.

Souza, A., E. Cutrim and J. Moraes, 1980: Variabilidade das Precipitacoes na Ilha de Marajo. Projeto Avaliacao e Utilizacao dos Recursos Hidricos da Ilha de Marajo, Relatorio Interno, NCGG, Univ. Fed. de Para, Belem, Brazil.

Staff Members, Institute of Tropical Meteorology (Poona), 1964: Meso-scale study of rainfall over Poona and neighborhood. *Indian J. Meteor. Geophys.,* **15,** 537–546.

Stout, J. E., D. W. Martin and D. N. Sikdar, 1979: Estimating GATE rainfall with geosynchronous satellite images. *Mon. Wea. Rev.,* **107,** 585–598.

Suomi, V. E., R. Fox, S. S. Limaye and W. L. Smith, 1983: McIDAS III: A modern interactive data access and analysis system. *J. Appl. Meteor.,* **22,** 766–778.